Active vibration control over the flexible structure of a kitchen hood

Fabio Previdi [a,*], Cristiano Spelta [a], Matteo Madaschi [a], Damiano Belloli [a,b], Sergio M. Savaresi [b], Francesco Faginoli [c], Enrico Silani [d]

[a] Dipartimento di Ingegneria, Università degli Studi di Bergamo, viale Marconi 5, 24044 Dalmine, BG, Italy
[b] Dipartimento di Elettronica, Informazione e Bioingegneria, Politecnico di Milano, P.zza L. da Vinci 32, 20133 Milano, Italy
[c] Laboratorio R&D, Faber spa, viale XIII luglio 160, 60044 Fabriano, AN, Italy
[d] CEFRIEL, via Fucini 2, 20133 Milano, Italy

Received 12 October 2013
Accepted 21 January 2014
Available online 16 February 2014

1. Introduction

Of many different types of actuators for active vibration suppression in flexible structures, piezoelectric (PZT) transducers are considered the best compromise among achievable performances, costs and reliability (see e.g. [5,7,11,31,13,27,34,1,29]).

Piezoelectric materials are sensitive to electric fields due to the permanent dipole of their crystal structure [22]. This kind of material strains when exposed to a voltage and provides a voltage when strained. So, in the first case, it can be used as an actuator, while in the second case it can be used as a sensor. The piezoelectric material is usually manufactured as a film and cut in small patches which can host both sensing and actuation on the same device.

The vast research activity of the last two decades devoted to piezoelectric materials can be divided into two mainstreams: the study of the material properties and behaviors (see e.g. [15,18,26]) and the research about control techniques and applications of devices based on piezoelectric materials (see e.g. [4,12,17,32,23,25]). This work belongs to the latter group.

For mechanical vibration reduction, piezoelectric patches can be used in either active control systems or passive ones. In a typical active control application, a piezoelectric patch actuates forces over a flexible structure while vibrations are measured by an appropriate sensor which is usually embedded in the actuator or collocated with it (see e.g. [10,2,36]). This approach is frequently used on a small flexible structure (the case of the present paper) where the problem of sensor/actuators placement is less critical than in the case of a large structure (for some example see [1,28]) The passive approach consists in the use of piezoelectric actuators shunted to a passive electric circuit that converts mechanical energy into electricity: so, the passive piezo-circuit system provides an extra-damping to the mechanical system (for some examples see [38,16]).

However, any passive framework can be emulated by an active control, which may also guarantee fine tuning on the vibration frequency, therefore achieving better performances. This is paid in terms of control design complexity, since only a passive framework is ensured to be stable with respect to any adopted configuration.

* Corresponding author. Tel.: +39 035 205 2004.
E-mail address: previdi@unibg.it (F. Previdi).

This paper deals with a control application of piezoelectric actuators for mechanical vibration suppression using an active control scheme. In particular, this study is focused on the use of a collocated piezoelectric patch and an accelerometer sensor for vibration and noise reduction in a kitchen hood (Fig. 1). As a matter of fact, the vibration reduction in a kitchen hood is extremely important since it directly affects the perceived noise. Actually, a low noise level is probably the most significant quality factor in kitchen hoods, together with design.

Roughly speaking, the noise produced by the hood has two main sources:

- The electric motor, which generates a mechanical vibration (@50 Hz and multiples) that is directly transmitted to the hood structure and produces an annoying single tone noise with high intensity.
- The turbulent motion of the air flowing inside the chimney, which causes a broad-band aerodynamic noise with low intenstity.

The aim of this work is the suppression of the most tiresome component of the noise, i.e. the one due to the mechanical vibration of the hood produced by the electric motor. To this aim, an active vibration control system has been designed using a piezoelectric actuator to contrast the hood wall vibration measured by a collocated accelerometer. The control design has been carried out according to the Generalized Minimum Variance (GMV) approach [39,40,8,14]. This method has been chosen for two main reasons: it can easily accommodate adaptive control strategies, and it can accomplish control action penalization. The first feature has been exploited to adaptively tune the controller parameters depending on the motor speed. The second one is very important in piezoelectric based control systems to avoid the use of excessive control energy. More specifically, a broad-band Minimum Variance controller is able to provide the theoretically best performance in terms of noise reduction, by deleting noise (no matter its source) over a given bandwidth. On the other side, a single-tone Minimum Variance controller (resonant controller) will provide noise cancellation only at given frequency values, selectively deleting only the noise due to the motor vibration. This approach is of particular interest in view of the use of soundproof materials to reduce aerodynamic noise. At the best of our knowledge, this paper contains the following innovative contributions:

- The topic of vibration reduction with PZT actuator in a kitchen hood has never been explored. To this aim a description of the experimental set-up and a control-oriented model of the system are provided.

Fig. 1. The kitchen hood object of this work.

- A vast experimental activity has been carried out and here reported in order to assess the effectiveness of the proposed control system. Final tests have also been held in an anechoic chamber to explore the relationship between the reduction in terms of vibration and in terms of noise.

The paper is organized as follows: the control system and the experimental set up are presented in Section 2. The model of the plant and the mathematical description of the disturbance are reported in Section 3. The control design and experimental tests of two active resonant control laws are described in Section 4, where some tests in an anechoic chamber are also reported. Finally, Section 5 contains some conclusive remarks.

2. Plant description

The kitchen hood used in this work is a prototype designed by Faber S.p.A. – Italy (Fig. 1). Such hood model is composed of two main parts, described in Fig. 2:

- The *external part*, including the chimney, the hood base and the air filters.
- The *internal part*, called "motor-box" (the grey part in Fig. 2), which is fixed to the back side of the external structure. The motor-box is made of a small fan and an electric motor encapsulated in a cubic box.

As commonly used in domestic appliances, the hood is equipped with a universal AC-motor fed by the public power network. As a consequence, the main rotation frequency of the motor is 50 Hz (European standard). The motor speed can be controlled by a triac, which saturates, at adjustable values, the input current to the motor. This way the modulation of the motor speed can easily be obtained. Unfortunately, current saturation introduces pure-tone disturbances (at frequencies in multiples of 100 Hz, such as 100 Hz, and 200 Hz) in the torque delivered by the electric motor. This disturbance is at the origin of the motor induced vibrations.

The control system uses a piezoelectric actuator to contrast the hood wall vibration on the basis of its measurement performed by an accelerometer. Notice that, for control purposes, the sensor is collocated with the actuator.

The piezoelectric actuator used in this project is a P876-A15 DuraAct Patch produced by PI Ceramic (Germany, Fig. 2). The actuator is characterized by the following features that make it appropriate for this kind of application: a maximum holding force of 775 N and a −250 V to +1000 V operating voltage. The patch is driven by a voltage amplifier designed by PI which is governed by a −5 V to +5 V analog voltage signal and delivers to the patch a control action in the −250 V to +750 V range over a bandwidth of 5 kHz with a power consumption up to 48 W.

Vibrations are measured by a ±50 g accelerometer designed and distributed by PCB Piezotronic and featuring a 0.2 Hz–20 kHz bandwidth.

The experimental final control loop is depicted in Fig. 3:

- The hood vibration $a(t)$ is measured by the acceleration transducer. The resulting voltage signal is then electronically conditioned (amplified and translated) as $a_c(t)$ and sampled by the ECU at a 10 kHz frequency.
- The ECU is a fast-prototyping system MicroAutobox by dSPACE, which runs at a control frequency of 10 kHz. The control unit computes the driving voltage $v^{\#}(t)$ according to the designed control law. The ECU is also responsible for the data logging.
- The sampled-and-hold output of the ECU is electronically conditioned and then amplified by the PI driver as the command signal $v_a(t)$.

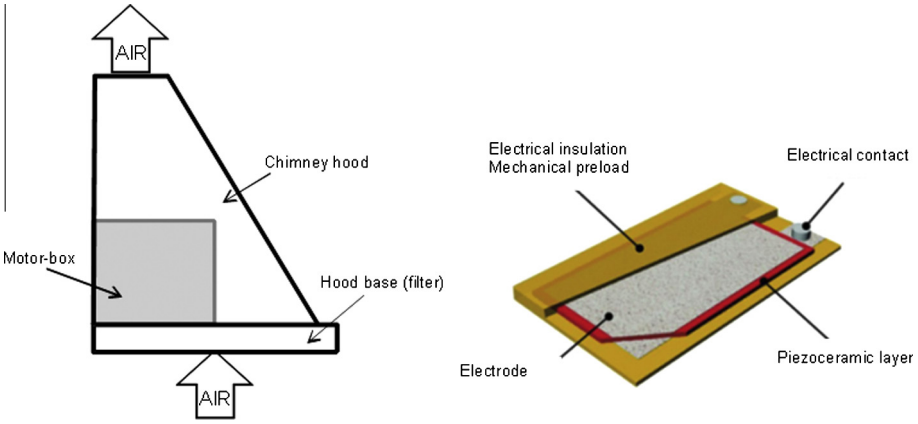

Fig. 2. Simplified scheme of the hood (left) and graphical description of the PZT patch (right).

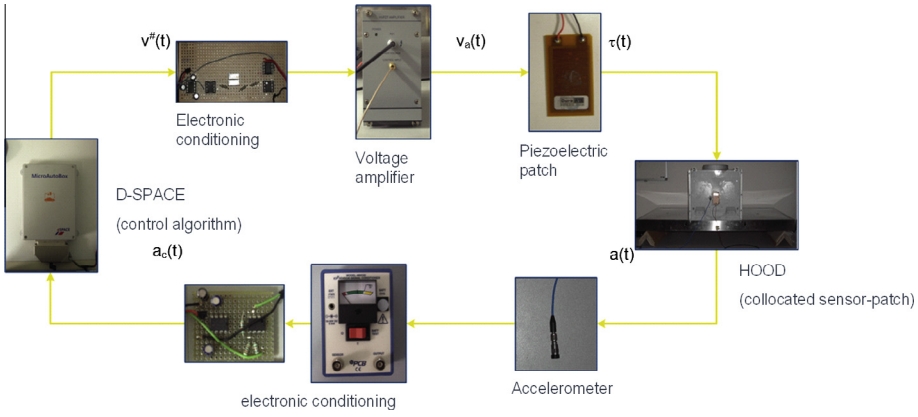

Fig. 3. Experimental set-up: control loop scheme.

- The voltage $v_a(t)$ drives the piezoelectric patch, which delivers a torque $\tau(t)$ on the hood surface.

3. Vibration measurements and Characterization of the system

The aim of this section is to present the performance evaluation metrics for vibration measurements and to characterize the vibrations' intensity of the hood structure.

The performance evaluation is carried out according to the following two indexes:

- The spectral density of the measured accelerations of the sensor-actuator pair $a_c(t)$, namely $A(\omega)$, where ω is a frequency where the spectral density is evaluated.
- The total cumulative sum of the acceleration spectral density, namely $\Gamma(\omega) = \int_0^{\omega} A(\omega)d\omega$. Notice that this second index is a measure of the energy in the acceleration signal up to frequency ω.

Both indexes $A(\omega)$ and $\Gamma(\omega)$ are computed by assuming 60 s experiments with 10 kHz sampling frequency (namely 600.000 samples per minute).

An example of a vibration intensity evaluation (results of an experiment with medium motor speed with sensor/actuator on the motor-box side – see Fig. 4) is reported in Fig. 5, which depicts both $A(\omega)$ and $\Gamma(\omega)$ over a frequency domain up to the Nyquist frequency of the sampled measurements (namely 5 kHz). From Fig. 5 it can be easily argued that the largest part of the vibration energy (about 90%) is concentrated below 500 Hz, as experienced in other similar applications (see for instance [29]. See also [20,21] for other interesting applications of spectral analysis techniques).

To obtain a complete characterization of the vibration intensity in different positions and speed conditions, several experiments have been performed. Specifically, the dependence on the sensor/actuator position has been evaluated over a grid of 10 points for each side of the hood (left side; right side; motor-box side – see

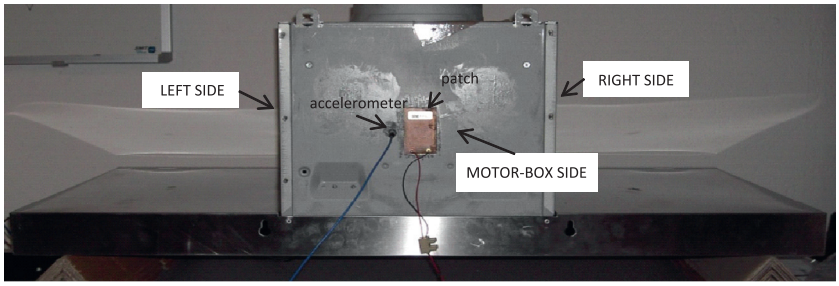

Fig. 4. Positioning of the sensor-actuator pair.

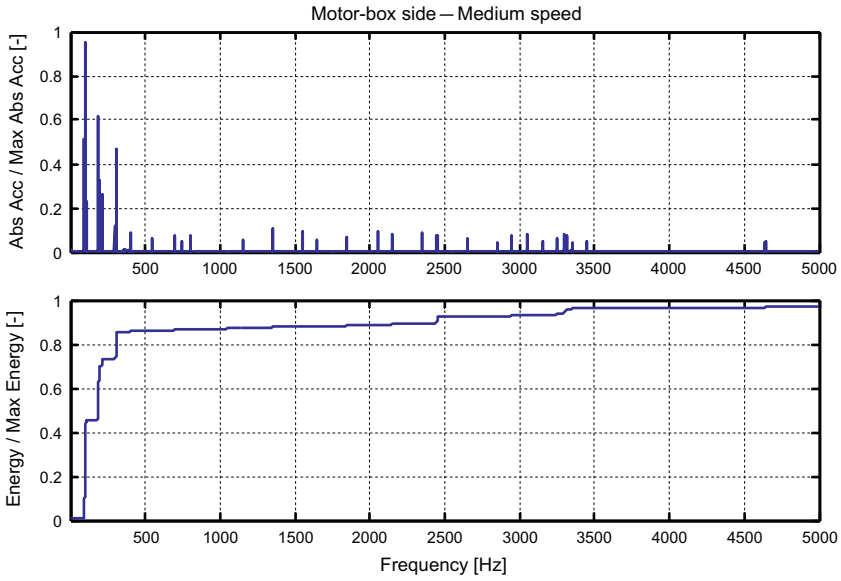

Fig. 5. Example of vibration evaluation. In detail: spectral density $A(\omega)$ of acceleration signal $a_c(t)$ (top) and cumulative sum of spectral density $\Gamma(\omega)$ (bottom).

Fig. 4). The position of the sensor/actuator pairs depends also on feasibility reasons. Basically, in view of industrial applications, they must be places on the motor-box side. Also, as expected, the vibrations are higher close to the motor-box and the controllability is better the closer to the motor-box are the actuators. The effect of the motor speed has been evaluated by experiments at the three available speed values (small, medium and large). The results of the position/speed analysis are shown in Fig. 6, where the frequency analysis has been limited to 500 Hz (see again Fig. 5).

By inspecting Figs. 5 and 6 some conclusions may be drawn:

- The spectral density plot $A(\omega)$ shows a finite number of significant resonant modes. The 100 Hz mode is usually dominant over all the others. Other high power harmonic components are visible at about 200 Hz and 300 Hz. These resonant modes are excited by the triac motor speed control. Interesting enough, the 50 Hz, 150 Hz, etc. modes are not as evident as the 100 Hz one (and multiples). This is not surprising as the hood structure has its proper resonant modes at about 100 Hz and multiples (as discussed in the next section).
- Close to the resonant frequencies in multiples of 100 Hz, other modes are clearly visible, produced by the modulation of the motor rotation frequency. These modes are not so evident in $A(\omega)$ since little energy is concentrated at that frequency. For instance, at medium speed, the nominal motor rotation frequency is about 10 Hz. Thus, other modes appear in correspondence of each primary peak $\bar{\omega} : \bar{\omega} + 10$ Hz (e.g. 110 Hz) and $\bar{\omega} - 10$ *Hz* (e.g. 90 Hz). This phenomenon has been observed at any rotation speed.
- As previously noticed and as evidenced by Fig. 5, the 90% of the vibration energy is concentrated in the frequency range 0–500 Hz, where the main resonances of the system can be found. For this reason, in the remaining part of the paper, the analysis will be focused over the frequency range 0–500 Hz.
- The vibration energy measured at the motor-box side position is overall four times as large as the one measured on either the left or right position. In fact, the motor-box, which is the main vibration source, is attached to the back panel of the hood (the "motor-box" side). Similarly, the vibration energy measured at medium motor speed is about twice as much than at the other two possible speed values. So, the motor side position at medium motor speed is the most promising and challenging experimental condition in terms of vibration suppression.

Following these observations, a simplified approach has been adopted (which is consistent with the proposed control-oriented perspective) based on linear modeling and control of collocated actuator-sensor, as detailed in the next sections.

4. Plant dynamic model

Due to the collocated sensor-actuator layout, the plant considered in this work can be effectively modeled by a linear system with two inputs and a single output [26,19,11]:

- The input $V_a(t)$ is the voltage driving the piezoelectric actuator (measurable control action).
- The second input $w(t)$ is the motor vibration (a non-measurable disturbance).
- The output is the acceleration $a(t)$ associated with the hood vibration (the controlled variable).

The measured acceleration can be viewed as the superimposition of the effects of the piezoelectric voltage command $V_a(t)$ by the transfer function $G_{aV}(s)$, and of the disturbance $w(t)$ by $G_{aw}(s)$, namely

$$a(t) = G_{aV}(s)V_a(t) + G_{aw}(s)w(t)$$

4.1. Collocated sensor-actuator model

As the accelerometer sensor and the piezoelectric actuator are collocated and fixed on a flexible structure, the transfer function $G_{aV}(z)$ can be modeled as follows [26,19,11]:

$$G_{aV}(s) = e^{-s\tau}s^g \left(\sum_{i=1}^{M} \frac{\gamma_i}{s^2 + 2\xi_{ri}\omega_{ri}s + \omega_{ri}^2} \right) \tag{1}$$

where $M \to \infty$ and $\gamma_i \geqslant 0$.

Eq. (1) describes the elastic response of the vibrating structure to an exciting input signal generated by a piezoelectric actuator. Notice that, practically, M is a finite number, arbitrary large, which represents the number of vibrating modes considered in the model. The condition $\gamma_i \geqslant 0$ holds since the sensor and the actuator are collocated [17]. Notice that $\gamma_i = 0$ only if the sensor and the actuator are positioned where the i-th mode is unobservable. The parameters ω_{ri} and ξ_{ri}, represent the natural frequency and the

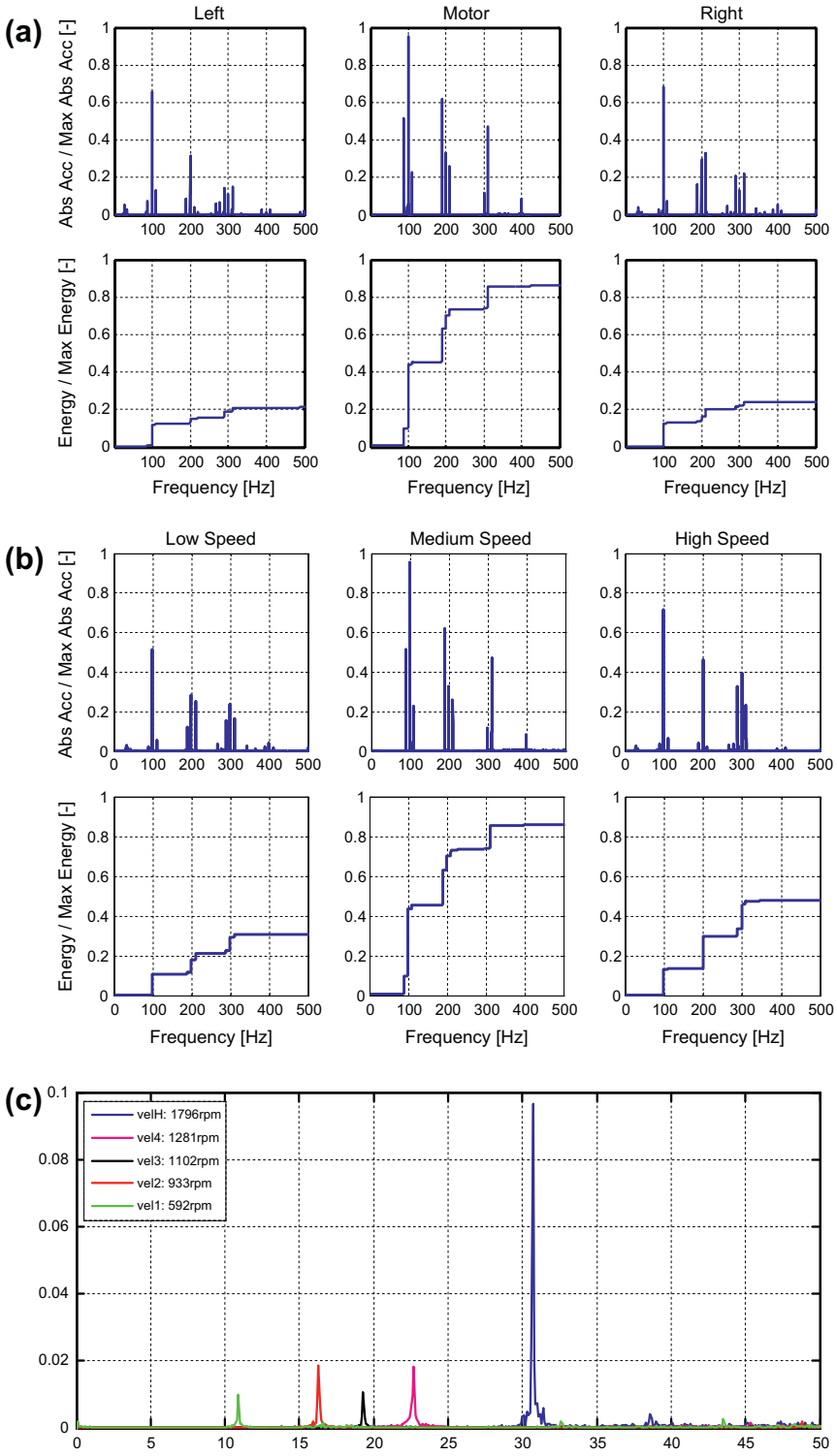

Fig. 6. Comparative analysis of the vibration intensity in three different positions over the hood structure (a) and at three different fan speeds (b). Top and bottom figures represent the spectral density $A(\omega)$ and the overall energy associated $\Gamma(\omega)$, respectively. In (c) the changes in the frequency of the first mode depending on the fan speed.

damping of the i-th vibrating mode of the flexible structure, respectively. Notice that the model of Eq. (1) includes a derivative contribution of order g. In fact, as already described, the piezoelectric material strains when a voltage is applied. This induces a deformation of the flexible structure where the patch is mounted. The deformation is measured by an accelerometer, so that the dynamical relation between the applied voltage and the monitored acceleration includes, usually, a double derivative contribution, namely s^2.

The parameters of Eq. (1) have been estimated by identification in the frequency domain. Specifically, a measurement of the frequency response $G_{aV}(j\omega)$ has been obtained by applying a sinusoidal sweep voltage signal with linearly increasing frequency from 5 to 500 Hz. Then, the model parameter values have been estimated by a two-step procedure:

- First, a structural identification issue has been tackled, aiming at estimating the vibrating mode number M.

- Second, for the estimated value of M, the remaining parameters have been tuned by minimization of the variance of the error between the experimental and the simulated frequency response data.

The results of the identification procedure are reported in Table 1 and depicted in Fig. 7, where the experimental and simulated Bode plots are compared. By inspecting Fig. 7 it can be noticed that the structural identification procedure captures three main poorly damped resonant modes (101 Hz, 147 Hz and 192 Hz) in the considered frequency band. Notice that, as already pointed out, the main harmonic component of the motor disturbance occurs at 100 Hz. High order modes are not visible due to both the sensor characteristics and the limit of the identification method, the sinusoidal sweep. In fact, it is known that, as the input signal frequency increases, the signal to noise ratio falls, and the identification accuracy is low. This is usually acceptable in control applications where high frequency model accuracy is not necessary.

4.2. Disturbance model

The transfer function $G_{aw}(s)$ describes the effect of an external non-measurable disturbance $w(t)$ on the hood. On the assumption that $w(t)$ is a white noise with zero mean and unitary H_2 norm, $G_{aw}(s)$ can be written as the sum of a set of poorly damped resonant filters describing the multi-tone disturbance, i.e. the vibration source:

$$G_{aw}(s) = \sum_{i=1}^{N} \alpha_i \frac{s^2 + 2r_i\omega_{di}s}{s^2 + 2r_i\omega_{di}s + \omega_{di}^2} \tag{2}$$

where ω_{di} is the i-th frequency of the multi-tone disturbance, as experimentally measured. The parameters r_i and α_i are obtained by minimization of the error's variance between the experimental and the simulated data. The results of the identification procedure are reported in Table 2 and represented in Fig. 8, where the experimental and the simulated spectral densities of the output of $G_{aw}(s)$ are compared. Notice that the values of the parameters r_i, $i = 1, \cdots, 8$ are practically negligible, as expected.

Table 1
Parameters of the resonant modes of the Model $G_{aV}(s)$.

Parameter	Estimated value
M	3
g	2
τ	0.0023 s
ω_{r1}, ξ_{r1}; γ_1 (1st mode)	0.63 krad/s (101 Hz); 0.030; 0.1781
ω_{r2}, ξ_{r2}; γ_2 (2nd mode)	0.93 krad/s (147 Hz); 0.025; 0.1102
ω_{r3}, ξ_{r3}, γ_3 (3rd mode)	1.21 krad/s (192 Hz); 0.025; 0.8130

5. Control design and results

In this section, the control algorithms design will be outlined according to the Generalized Minimum Variance (GMV) approach. We decided to start with a SISO architecture, leaving the investigation of the MIMO approach to future work. One of the reason is practical industrial feasibility of the system, which cannot use more than a couple sensor/actuators for cost reasons. Moreover, the main vibration source is on the motor box side and it is wise to start our preliminary analysis on that side only.

We used GMV because it is the discrete time optimal predictive control for linear systems affected by noise. Moreover, GMV is a 2-DOF controller that will have an easy implementation in view of adaptive control. Finally, GMV allows parsimonious control by introducing penalization of the control action in a very easy way. So, we decided to use a broadband GMV controller as a starting point for our analysis.

5.1. Broad-band GMV controller (BB-GMV): the benchmark

For control design and implementation purposes the measured acceleration is sampled $y(k) = a(kT)$, where $f_s = \frac{1}{T} = 20$ kHz is the sampling frequency. Similarly, discrete time sampled transfer functions of the model are computed by the use of Tustin

Table 2
Parameters of model $G_{aw}(s)$.

Parameter	Estimated value
N	8 (Experimentally observed)
ω_{d1}, r_1; α_1 (1st tone)	0.56 krad/s (90 Hz); 0.0001; 0.0003
ω_{d2}, r_2; α_2 (2nd tone)	0.63 krad/s (100 Hz); 0.0001; 0.0013
ω_{d3}, r_3, α_3 (3rd tone)	0.69 krad/s (110 Hz); 0.0001; 0.0004
ω_{d4}, r_4, α_4 (4th tone)	1.19 krad/s (190 Hz); 0.00015; 0.0016
ω_{d5}, r_5, α_5 (5th tone)	1.26 krad/s (200 Hz); 0.00008; 0.0008
ω_{d6}, r_6, α_6 (6th tone)	1.32 krad/s (210 Hz); 0.00008; 0.0008
ω_{d7}, r_7, α_7 (7th tone)	1.88 krad/s (300 Hz); 0.00008; 0.0006
ω_{d8}, r_8, α_8 (8th tone)	1.95 krad/s (310 Hz); 0.0001; 0.0019

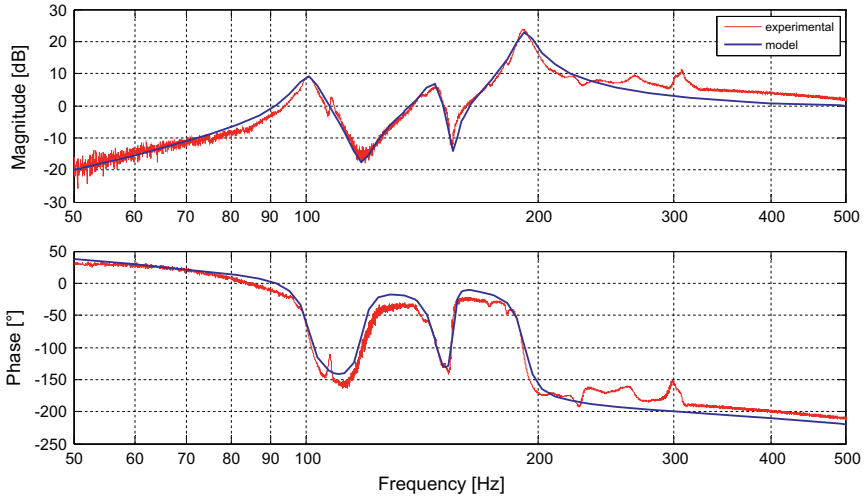

Fig. 7. Comparison between the experimental and the estimated Bode plots of $G_{aV}(s)$.

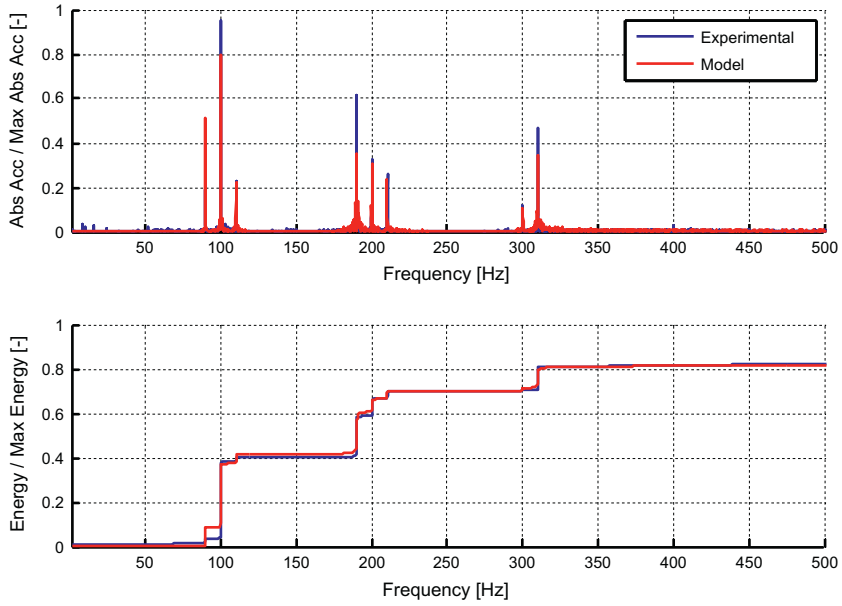

Fig. 8. The spectral density and the overall associated energy of the accelerations induced by the disturbance. Comparison between estimated (red) and measured data (blue). (For interpretation of the references to colour in this figure legend, the reader is referred to the web version of this article.)

transform, namely the disturbance model $\widetilde{G}_{\tilde{a}\xi}(z)$, being $\xi \approx \mathrm{WGN}(0,\lambda^2)$, and the plant model $\widetilde{G}_{a\widetilde{V}}(z)$, being $u(k) = V_a(kT)$. As represented in Fig. 9, through an appropriate algebraic manipulation, the plant may be described by an ARMAX model as follows:

$$A(z)y(k) = B(z)u(t-d) + C(z)\xi(k) \tag{3}$$

with $\xi(\cdot) \sim WGN(0,\lambda^2)$.

The GMV ARMAX-model-based control law $u(k)$ is designed by minimization of the following cost function:

$$J = E[(P(z)y(k+d) + Q(z)u(k) - y^0(k))^2] \tag{4}$$

where

- $y^0(k)$ is the reference trajectory to be tracked;
- $P(z)^{-1} = \frac{P_D(z)}{P_N(z)}$ is a reference model for the closed loop system;
- $Q(z) = \frac{Q_N(z)}{Q_D(z)}$ is a weight filter penalizing the use of large control energy.

It can be proven that, under mild assumptions on the filters $P(z)$ and $Q(z)$ (see Astrom, 1970; [14], the optimal controller is 2-DOF and is given by the following equations:

$$G(z)u(k) = H(z)y^0(k) - F(z)y(k) \tag{5}$$

where

$$G(z) = P_D(z)[B(z)Q_D(z)E(z) + C(z)Q_N(z)] \tag{6.a}$$

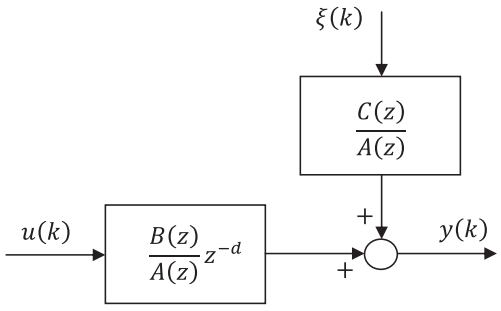

Fig. 9. Discrete time model of the plant.

$$F(z) = \widetilde{F}(z)Q_D(z) \tag{6.b}$$

$$H(z) = C(z)P_D(z)Q_D(z) \tag{6.c}$$

being $E(z)$ and $\widetilde{F}(z)$ defined, respectively, as the solution and the remainder of the following Diophantine equation:

$$P_N(z)C(z) = P_D(z)A(z)E(z) + z^{-d}\widetilde{F}(z) \tag{7}$$

It is worth noting that in the present case, the peculiarity of the control problem allows a significant simplification of the above equations. In fact:

- The reference acceleration is $y^0(k) = 0$; so, it is not necessary to compute Eq. (6.c), because Eq. (5) reduces to $G(z)u(k) = -F(z)y(k)$.
- Since the aim is perfect rejection of the resonant mode, a unitary reference model has been chosen, so $P_N(z) = P_D(z) = 1$ and Eq. (7) simply become $C(z) = A(z)E(z) + z^{-d}\widetilde{F}(z)$.
- Using a constant penalization of the control action, i.e. $Q_N(z) = q$ and $Q_D(z) = 1$, $F(z)\widetilde{F}(z)$ and $G(z) = B(z)E(z) + qC(z)$ are obtained in Eqs. (6.a) and (6.b).

By plugging a full plant model with disturbance (1) and (2) into Eq. (3), and by solving Eqs. 5, 6.a, 6.b, 6.c, 7, it is possible to compute the BB-GMV controller for the hood. The results on the vibration suppression are reported in Fig. 10, and obtained in simulation by using experimental signals.

By inspecting Fig. 10 it is evident that the BB-GMV controller is able to suppress the structural harmonics of the hood (100, 200 and 300 Hz), while it is less effective on those harmonics that are due to motor speed disturbances. Overall the vibration suppression is around 95%, and the resulting closed loop vibration presents an almost flat spectrum, which is typical of a white noise. Under this perspective, due to optimality, this closed loop system represents a benchmark hard to be overcome for any other control strategy (with the same set of sensors and actuators).

However, as experimentally proven, this kind of controller cannot be implemented, since unstable behaviors arise. This is not surprising since at the 300 Hz mode, the transfer function from the control action to the vibration measure G_{aV} shows a phase-shift

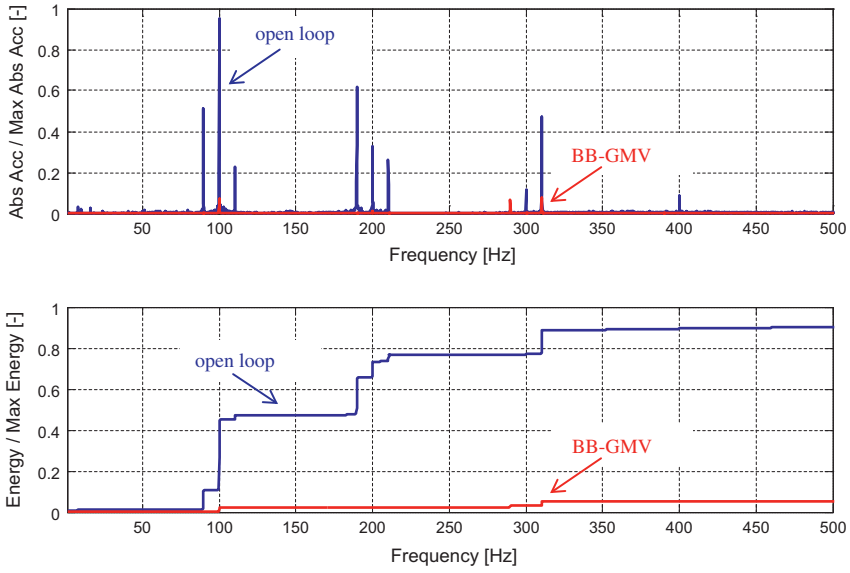

Fig. 10. Vibration evaluation for an open loop system and a closed loop system controlled by a broad-band generalized Minimum Variance controller (BB-GMV).

of about 180°, which represents a critical limit for the stability of the closed loop system (see Fig. 7).

5.2. GMV resonant controllers

In order to ensure stability for the closed loop system, two kinds of GMV resonant controllers are herein proposed.

As well known in active vibration control, it is possible to design the controller by exploiting the peculiar nature of the disturbance, which presents a number of poorly damped resonant poles. This allows the design of a resonant controller, which is able to guarantee unconditional stability of the closed loop system [4,6,24]. Resonant controllers are extremely effective when correctly tuned in correspondence of the disturbance modes [31].

In order to design a resonant GMV controller, first of all, consider the significant case of when the disturbance is a pure-tone undamped vibration with frequency $\bar{\omega}$. According to Eq. (2) the disturbance can be described, in a discrete time with a sampling period T, by the following transfer function:

$$\widetilde{G}_{\tilde{a}\xi}(z) \triangleq \frac{C(z)}{A(z)} = \frac{1-(1+\cos(\bar{\omega}T))z^{-1}+\cos(\bar{\omega}T)z^{-2}}{1-2\cos(\bar{\omega}T)z^{-1}+z^{-2}} \tag{8}$$

At frequency $\bar{\omega}$, according to the theorem of frequency response, the plant model can be described by a gain μ and a time delay $\tau = d{\cdot}T$. In this setting, it is possible to solve the Generalized Minimum Variance problem for every frequency of interest. Then the resulting controller is the sum of the single resonant controllers so designed.

Finally, two kinds of resonant controllers are herein proposed in such a way:

- A Simplified Resonant Controller (SRC-GMV), which acts without the information of the motor speed velocity and aims at suppressing the tones at 100 Hz, 200 Hz and 300 Hz.
- A General Resonant Controller (GRC-GMV), which exploits the information on the motor speed velocity. In this situation it is possible to act on the structural tones at 100 Hz and multiples, and further on those frequencies related with the motor disturbance (e.g. if the motor disturbance is at 10 Hz, then the other harmonics due to modulation are at 90 Hz, 110 Hz, 190 Hz, 210 Hz, 290 Hz, and 310 Hz). Notice that the hood's motor is not provided with a velocity sensor. Therefore, the control scheme must include an on-line estimation procedure of the motor rotation speed (see Fig. 11). In this work, an adaptive notch filter has been used, designed according to the algorithm in [30]. For the sake of honesty, it is worth saying that in literature many algorithms can be found to tackle the rotation frequency estimation problem (see for instance [9,37,33,35] and references cited therein). The final framework of the GRC-GMV, with an on-line adaptation of the motor speed velocity, is depicted in Fig. 11.

5.3. Experimental results

The resonant controllers previously designed have been implemented in the fast prototyping ECU (dSPACE) and experimentally evaluated. The comparison is made with respect to the open loop system and the closed loop with BB-GMV (simulated). Figs. 12–14 collect the results. Some conclusions may be drawn:

- GRC-GMV is able to effectively reject the disturbance tones of vibrations. It is comparatively less effective at the harmonics of the motor disturbance. Overall the reduction of the vibrations' level is around 85% when compared to an open loop configuration. The degradation compared to the BB-GMV controller (simulated) is around 5%. This makes the GRC-GMV an

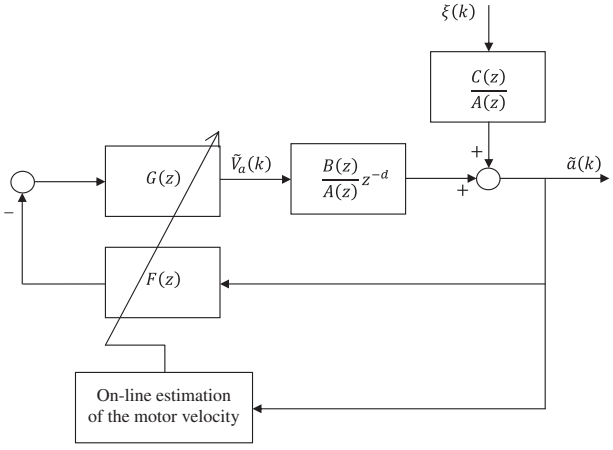

Fig. 11. Scheme of the GRC-GMV controller including the motor speed estimation algorithm.

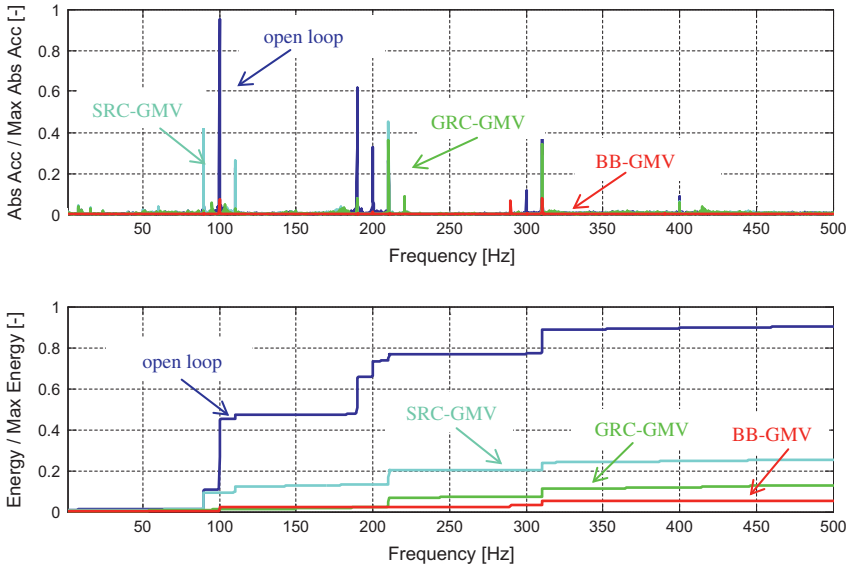

Fig. 12. Experimental vibration evaluation for an open loop system and a closed loop system with GRC-GMV and SRC-GMV controllers, compared to the lower bound provided by BB-GMV controller.

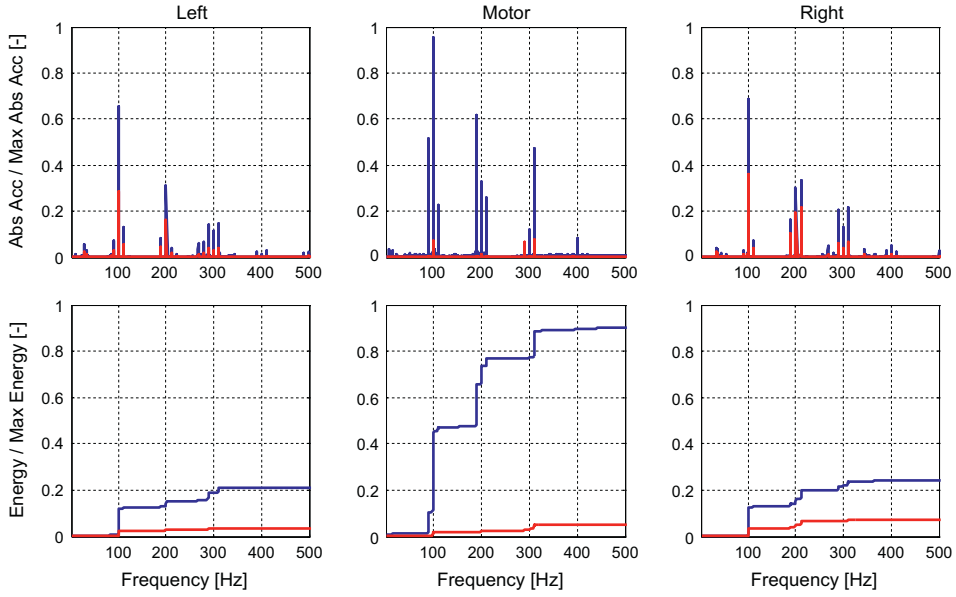

Fig. 13. Experimental vibration evaluation in three different hood positions: with the sensor/actuator placed on the motor side, for an open loop system (blue) and a closed loop system with GRC-GMV controller (red). Vibrations are significantly reduced also on the other sides of the hood. (For interpretation of the references to colour in this figure legend, the reader is referred to the web version of this article.)

implementable good approximation of optimal controller (BB-GMV) for vibration suppression. This is paid in terms of complexity of the motor speed velocity's on-line estimation.

- The SRC-GMV is simpler because of the presence of only three harmonics to reject. The simple layout is paid in terms of overall performance. The reduction of vibrations is around 75%, with a degradation of about 15% with respect to the optimal BB-GMV controller.
- With both controllers the harmonics at 100 Hz, 200 Hz, and 300 Hz, are fully suppressed with a reduction of 55db (600 times less) of the spectrum in correspondence of those tones. The control is less effective on those harmonics that arise due to the non-linear nature of the system.
- Positioning the actuator/sensor close to the motor-box produces a significant vibration reduction also on the other sides of the hood (see Fig. 13).

This section is concluded with the results about some tests held in the anechoic chamber to show how the reduction of vibration may influence the perceived acoustic noise. The test facility is located at the Sound Laboratory of the R&D department of Faber S.p.A. at Fabriano (Ancona – Italy).

The acoustic noise is measured as the pressure variation of the air by a microphone. The measured signal is sampled at 1 MHz and then processed by a real time sound level meter. While the microphone has an approximately constant gain on a large frequency range, this is not the case of the human ear. Specifically, the human ear is significantly less sensitive to lower frequencies, up to about 1 kHz. So, the sound analyzer weights the measured data through the so called inverse isophonic curve "A", which emulates the human ear reaction to perceived sounds with different frequencies. The analyzer provides a sound level index, usually represented in logarithmic scale and expressed in dBA.

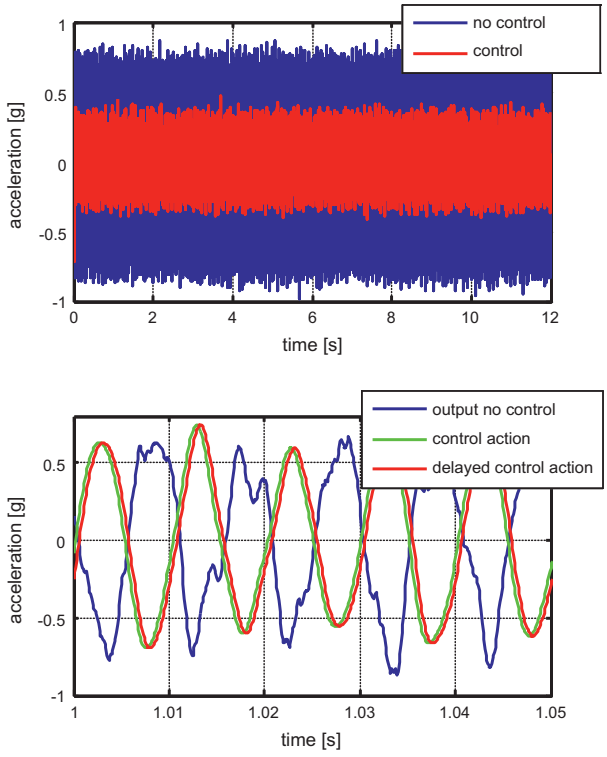

Fig. 14. Measurement of acceleration in time domain. In the upper figure, the effect of the closed loop control on the vibration amplitude. In the lower figure, the control action without delay and with the optimal delay.

From Fig. 15, the following conclusions can be drawn:

- The bandwidth of the acoustic noise is significantly much wider (up to 4 kHz) than the bandwidth of the vibration disturbance. In fact, the acoustic noise is mainly of aerodynamic origin (the air passing through the hood filter and chimney). As a consequence, the activation of control mainly reduces noise at about 100 Hz where a reduction of almost 6 dB is registered.
- The test confirms that the reduction of vibrations has an influence upon the acoustic noise in the frequency range of interest, but the aerodynamics noise is much more important and, as expected, it is not affected by the control of the accelerations measured over the flexible structure. Some results in aerodynamic noise reduction might be obtained by feedback of a direct measure of the acoustic noise (genuine active noise control).

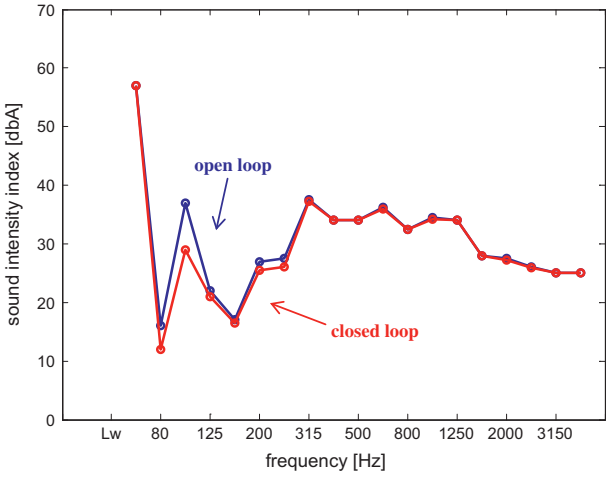

Fig. 15. Sound intensity index in dbA as measured in anechoic chamber. Comparison between open and closed loop systems. Notice that the sound intensity has been reduced in the interesting frequency range.

6. Concluding remarks

In this paper, the full analysis and development of a system for vibration reduction of a kitchen hood has been presented. The control system is an active feedback control based on voltage driven cost effective piezoelectric patches. Two kinds of resonant controllers have been designed, with or without considering the motor velocity information. For benchmarking purposes a broad-band generalized Minimum Variance controller has been designed and simulated. The effectiveness of both controllers has been shown. In particular, through the information about the motor speed, the best performances are guaranteed with a reduction of 85% of the vibrations (5% of degradation with respect to the benchmark). However, the resonant control system without the motor speed information seems to provide the best compromise in terms of performances and complexity of the implemented system (75% of reduction and 15% of degradation).

Finally, tests held in anechoic chamber have shown the influence of the vibration reduction upon the acoustic noise.

Future work can be performed in the direction of using the proposed method in the framework of classical control methods for collocated actuators and sensors, i.e. Integral Resonant Control (IRC – [3]. For instance it is advisable to develop a discrete time implementation and (possible) development of a tuning method based on Minimum Variance criterion for IRC. Also it could be developed an Adaptive Internal Resonance Control scheme by designing suitable scheduling algorithms, in order to fulfil the requirements of the present application, i.e. to have a controller dependent on the fan speed.

Acknowledgment

The authors would like to thank Maria G. Perrone, Bakersfield College (USA) faculty, for the useful language review.

References

[1] Allen M, Bernelli-Zazzera F, Scattolini R. Sliding mode control of a large flexible space structure. Control Eng Practice 2000;8(8):861–71.
[2] Anderson EH, Hagood N, Goodliffe JM. Self sensing piezoelectric actuations. Analysis and application to controlled structures. In: Proceedings of structures, structural dynamics, materials conference, Dallas (TX); 1992. p. 2141–55.
[3] Aphale SS, Fleming AJ, Moheimani SOR. Integral resonant control of collocated smart structures. IOP Smart Mater Struct 2007;16:439–46.
[4] Balas MJ. Feedback control of flexible systems. IEEE Trans Autom Control 1978;AC-23(4):673–9.
[5] Bianchini E, Spangler R. The use of piezoelectric devices to control snowboard vibrations. In: Proceedings of SPIE conference of integrated systems; 1998. p. 106–14.
[6] Bittanti S, Dell'Orto F, Di Carlo A, Savaresi S. Notch filtering and multirate control for radial tracking in high-speed DVD-players. IEEE Trans Consum Electron 2002;48(1):56–62.
[7] Casella F, Locatelli A, Schiavoni N. Modeling and control for vibration suppresion in a large flexible structure with jet thruster and piezoactuator. IEEE Trans Control Syst Technol 2002;10(4):589–99.
[8] Clarke DW, Gawthrop PJ. Self-tuning control. IEE Proc Control Theory Appl 1979;126(6):633–40.
[9] Dooley SR, Nandi AK. Fast frequency estimation and tracking using Lagrange interpolation. Electron Lett 1998;34(20):1908–10.
[10] Dosch J, Inman DJ, Garcia E. A self-sensing piezoelectric actuator for collocated control. J Intell Mater Struct 1992;3(1):166–85.
[11] Fuller CR, Elliot SJ, Nelson PA. Active control of vibrations. London: Academic Press Limited; 1996.
[12] Gani A, Salami MJE, Khan R. Active vibration control of a beam with piezoelectric patches: real-time implementation with xPC target. Proceedings of 2003 IEEE conference on control applications; 2003. p. 538–44.
[13] Garcia ED, Inman D, Dosch J. Vibration suppression using smart structures. In: Proceedings of smart structures materials conference; 1991. p. 167–72.

[14] Grimble MJ. Generalized minimum variance control law revisited. Opt Control Appl Methods 1988;9(1):63–77.
[15] Hagood N, Chung W, von Flotov A. Modeling of piezoelectric actuator dynamics for active structural control. J Intell Mater Syst Struct 1990;1(3):327–54.
[16] Hagood NW, Crawley EF. Experimental investigation of passive enanchement of damping for smart structure. AIAA J Guid, Navigat Control 1991;1(3):327–54.
[17] Halim D, Moheimani SOR. Spatial resonant control of flexible structures – application to a piezoelectric Laminate beam. IEEE Trans Control Sytem Technol 2001;9(1):37–53.
[18] He Z, Loh HT, Xie M, Guo G. A reliability model for piezoelectric actuators. In: Proceedings of 7th international power engineering conference, Singapore; 2005. p. 939–44.
[19] Hughes PC. Space structure vibration modes: how many exist? Which one are important? IEEE Control Syst Magaz 1987;7(1):22–8.
[20] Masini A, Batani D, Previdi F, Milani M, Pozzi A, Turcu E, et al. Yeast cell metabolism investigated by CO_2 production and soft X-ray irradiation. Eur Phys J – Appl Phys 1999;5(1):101–9.
[21] Previdi F, Parisini T. Model-free actuator fault detection using a spectral estimation approach: the case of the DAMADICS benchmark problem. Control Eng Practice 2006;14(6):635–44.
[22] Standard committee of the ultrasonics. Ferroelectrics and frequency control society. IEEE standard on piezoelectricity. ANSI/IEEE Standards; 1988.
[23] Jain S, Manjunath TC, Bandyopadhyay B. Active vibration control of glass-epoxy composite box beam using output feedback. In: IEEE international conference on industrial technology; 2006. p. 2200–05.
[24] Joshi SM, Gupta S. On a Class of marginally stable positive-real systems. IEEE Trans Autom Control 1996;41(1):152–5.
[25] Joujou MK, Mrad F, Smail A. Experimental fuzzy logic active vibration control. In: Proceedings of the 5th international symposium on mechatronics and its applications, Ammam (Jordan); 2008. p. 1–7.
[26] Juang J, Phan MQ. Identification and control of mechanical system. Cambridge: Cambridge University Press; 2001.
[27] Kermani MR, Moallem M, Patel RV. Parameter selection and control design for vibration suppression using piezoelectric transducers. Control Eng Practice 2004;12(8):1005–15.
[28] Kozek M, Benatzky C, Schirrer A, Stribersky A. Vibration damping of a flexible car body structure using piezo-stack actuators. Control Eng Practice 2011;19(3):298–310.
[29] Leva A, Piroddi L. FPGA-based implementation of high-speed active noise and vibration controllers. Control Eng Practice 2011;19(8):798–808.
[30] Li TH, Kedem B. Tracking abrupt frequency changes. J Time Ser Anal 1998;19(1):69–82.
[31] Moheimani S. A survey of recent innovations in vibrating damping and control using shunted piezoelectric transducers. IEEE Trans Control Syst Technol 2003;11(4):482–92.
[32] Moheimani SOR, Dunant H. Spatial resonant control with collocated piezoelectric actuator/sensor Pairs. In: Proceedings of the American control conference, Arlington, VA, USA; 2001. p. 1960–65.
[33] Naishan H, Wu J. A fast algorithm for frequency estimation of power systems in colored noises. In: IEEE southest conf, Fort Lauderdale, Florida (USA); 2005. p. 34–8.
[34] Preumont A. Vibration control of active structures – an introduction. Dordrecht, The Netherlands: Kluwer Academic Publishers; 2002.
[35] So HC, Ching PC. Adaptive algorithm for direct frequency estimation. IEE Proc Radar, Sonar Navigat 2004;151(6):359–64.
[36] Vallone P. High performance piezo-based self sensor for structural vibration control. In: Proceedings of SPIE conference on smart structures integrated systems; 1995. p. 643–55.
[37] Varadan VV, Wu Z, Hong SY, Varadan VK. Active control of sound radiation form a vibrating structure. In: IEEE Ultrasonics symposium; 1991. p. 991–4.
[38] Wu SY. Multiple PZT Transducer Implemented with multiple-mode piezoelectric shunt for passive vibrating damping. In: Proceedings of the SPIE symposium on smart structures materiales passive damping isolation; 1999. p. 113–22.
[39] Åstrom KJ. Introduction to stochastic control theory. New York: Academic Press; 1970.
[40] Åstrom KJ, Wittenmark B. On self tuning regulators. Automatica 1973;9(2):185–99.